Catalysis Today 166 (2011) 166–171

Contents lists available at ScienceDirect

Catalysis Today

journal homepage: www.elsevier.com/locate/cattod

Sonochemical deposition of silver–TiO_2 nanocomposites onto foamed waste-glass: Evaluation of Eosin Y decomposition under sunlight irradiation

S. Obregón Alfaro [a], V. Rodríguez-González [b,*], A.A. Zaldívar-Cadena [c], S.W. Lee [d]

[a] Facultad de Ingeniería Mecánica y Eléctrica, Universidad Autónoma de Nuevo León, Cd. Universitaria, C.P. 66451, San Nicolás de los Garza, N.L., Mexico
[b] IPICYT, Instituto Potosino de Investigación Científica y Tecnológica, División de Materiales Avanzados, Camino a la Presa San José 2055, Col. Lomas 4a. sección, C.P. 78216, San Luis Potosí, S.L.P., Mexico
[c] Facultad de Ingeniería Civil, Universidad Autónoma de Nuevo León, Cd. Universitaria, C.P. 66451, San Nicolás de los Garza, N.L., Mexico
[d] Department of Materials Engineering, Sun Moon University, Galsan-Ri, Tangjung-Myon, Asan Chungnam 336-708, South Korea

ARTICLE INFO

Article history:
Available online 31 July 2010

Keywords:
Sonochemical deposition
Silver photodeposited TiO_2
Polyvinyl alcohol
Coated foamed waste-glass
Eosin Y solar oxidation

ABSTRACT

TiO_2 and Ag–TiO_2 nanocomposites have been deposited on commercial foamed waste-glass strips (FWGS) by the sonochemical technique. The coated FWGS were characterized by scanning electron microscopy (SEM), high-resolution transmission electron microscopy (HRTEM) and energy dispersive X-ray spectroscopy (EDS). The addition of polyvinyl alcohol as surfactant to the sonochemical deposition process enhances the nanocomposite deposition, resulting in the formation of TiO_2 composites which are compact, uniform and adherent to FWGS. SEM images show that the oxides which were deposited consist of interconnected aggregates quasi-spheres ~25 nm in width. Energy dispersive spectroscopy data revealed oxides of TiO_2 formed onto the porous aluminosilicate. Surface morphology studies reveal randomly oriented aggregates with a raising structure around the pores with an average ~5 μm of diameter. The coated strips were evaluated for photoxidation of Eosin Y dye under sunlight. Experiments to evaluate the photocatalytic activity of supported TiO_2 were performed in common glass bottles under solar irradiation. Silver–titania-coated strips had the optimal performance, achieving 50% of mineralization and total Eosin Y solar discoloration.

1. Introduction

The anatase TiO_2 polymorph is the most important photocatalyst used today. Since the discovery of its photocatalytic activity by UV irradiation in 1972 [1], many studies have been developed with this material in the photodegradation of phenols [2], dyes [3], microorganisms [4], herbicides [5] and a variety of organic contaminants. Its band gap energy of 3.2 eV provides the formation of electron–hole pairs which may be activated with wavelengths shorter than 380 nm. Therefore, many efforts have been made to enhance the activation of TiO_2 at wavelengths closer to those of visible light. These efforts include methods such as doping of TiO_2 with transition metals, rare earths, metals, non-metallic anions, and surface modification (impregnation and deposition) with noble metals [6–9]. Regularly, surface modification consists of nanoparticles embedded or anchored to the surface of TiO_2, trapping of electrons being its main function, thereby decreasing the recombination of the electron–hole pairs. For noble metals, silver is one of the most suitable for industrial applications due to its low cost and ease of preparation. Nanoparticles of silver anchored to the surface of TiO_2 have proven to be highly efficient, favoring the activation of the titania under visible light irradiation [10–13].

Traditional technologies for wastewater treatment are often too expensive for practical applications. Today, the use of solar disinfection (SODIS) in conjunction with solar photocatalytic materials (TiO_2, for example) provides one of the most promising techniques for the remediation of wastewaters at low cost [14]. However, the application of this technique on a large scale is limited because of difficulties in the separation of TiO_2 suspensions from the system after the photoreactions take place. A possible solution for this problem is to immobilize the photocatalyst on a porous support. For this purpose, the ultrasound-assisted method was proven to be an interesting technique for deposition of photocatalysts on different supports [15–17]. The activity of ultrasound irradiation by acoustic cavitation phenomena involves the creation, growth, and implosive collapse of bubbles in the solution [18]. Consequently, this technique has been used for the deposition of different oxides into mesoporous materials and textile fibers [19].

In this work, it is presented a process for sonochemical deposition of silver–TiO_2 composite on a foamed waste-glass material. The deposition was developed by using polyvinyl alcohol as

* Corresponding author. Tel.: +52 444 8342000x7295; fax: +52 444 8342010.
E-mail addresses: vicente.rdz@ipicyt.edu.mx, vicenrg@hotmail.com (V. Rodríguez-González).

0920-5861/$ – see front matter © 2010 Elsevier B.V. All rights reserved.
doi:10.1016/j.cattod.2010.06.028

surfactant. The deposited coat on FWGS was characterized by FE-SEM and HRTEM microscopies. The evaluation of photocatalytic properties of the coated FWGS was carried out using as a model dye contaminant the Eosin Y dye (C.I. number 45380) under sunlight irradiation.

2. Experimental

2.1. Preparation of photodeposited silver–TiO_2 composite

The silver–TiO_2 (Ag/TiO_2) nanocomposite was prepared by a photodeposition technique. First, 0.407 g of $AgNO_3$ [Samchun Chemical Co., 99%] were added in 1 L of bidistilled water and placed in an ultrasonic bath for 5 min to assure the complete disaggregation of the silver precursor. Then, 25.0 g of titanium dioxide (P25, Degussa Chemical Co.) were added to the solution under vigorous stirring for 1 h in order to achieve the adsorption equilibrium of the Ag^+ ions on the TiO_2 surface. Afterwards, the mixture was irradiated with two 20 W UV C-type lamps (Black light lamp-BL, Sankyo Denky, Japan) for 2 h. The resulting silver–TiO_2 or TiO_2 was dried in a vacuum rotary evaporator at 80 °C for 4 h, and then at 100 °C in a vacuum oven for 12 h.

2.2. Sonochemical deposition of silver–TiO_2 over foamed waste-glass strips

The foamed waste-glass was provided by IPP Ltd., from South Korea. The dimensions of each strip use were 0.1 m × 0.01 m × 0.005 m; this size was designed according to the glass bottle dimensions use as a sunlight reactor system. The FWGS were pretreated by washing with bidistilled water in the presence of ultrasound frequency of 23.3 kHz for 2 h in order to remove any impurities of the FWGS. Then, the strips were coated with TiO_2 or silver photodeposited Ag/TiO_2 through the sonochemical process. 0.01 g of polyvinyl alcohol 500 (Junsei Chemical Co., Ltd., chemical pure grade) were added in 1 L of distilled water. This mixture was placed in a homemade ultrasound bath for 0.5 h to promote the dissolution of polyvinyl alcohol (PVA). Afterwards, there was added 1.0 g of silver–TiO_2 or TiO_2 composite and two strips of FWG. Then, the samples were sonicated for 2 h at 23.3 kHz, 800 W and a pressure of 8×10^{-2} MPa. The temperature was maintained at 20 °C with a cooling system. Subsequently, the strips were dried overnight at 60 °C under vacuum.

2.3. TiO_2 and Ag/TiO_2 deposition on foamed waste-glass strips characterization

Powder X-ray diffraction (XRD) measurements (Bruker D8 Advanced diffractometer, Cu Kα radiation, from 10° to 70°) were used to identify the crystalline phases of the Ag/TiO_2 and TiO_2 semiconductors. The crystallite sizes were calculated from the peak widths using the Scherrer equation: $D = k\lambda/\beta\cos\theta$, where D is the particle size, k is a constant (in this study $k = 0.89$), λ is the X-ray wavelength (1.5406 Å) and β is the half-width of the peak at 2θ. The samples were degassed for 12 h at 300 °C in vacuum prior to the measurements of the specific surface areas (BET method) and mean pore size diameter (BJH method), which were determined from nitrogen adsorption–desorption isotherms obtained with an Autosorb 3B apparatus (Quantachrome). UV–vis diffuse reflectance spectroscopy was performed by means of a Varian Cary 100 spectrometer with $BaSO_4$ coated integration sphere. The samples were placed in a Teflon cell (thickness of ~2 mm) to measure the remission function $F(R\infty)$. The silver–TiO_2 nanocomposites were characterized by a Philips TECNAI F30 field-emission transmission electron microscope (FE-TEM). The FE-SEM (PHILIPS XL 30S FEG) was used to characterize the morphology of coated strips. The coated strips were analyzed by an energy dispersive X-ray spectroscopy (EDS) detector coupled to the HR-STEM unit.

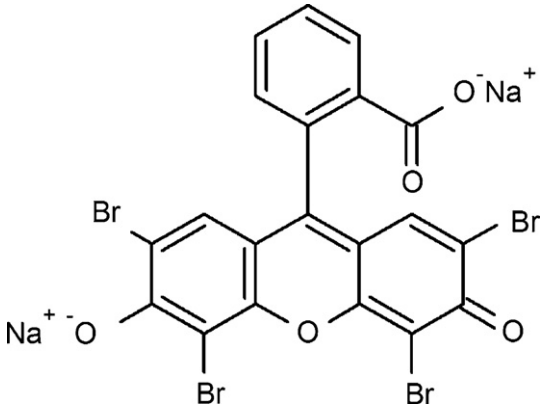

Fig. 1. Molecular structure of Eosin Y dye.

2.4. Sunlight oxidation of Eosin Y

The photocatalytic degradation of Eosin Y dye $C_{20}H_6Br_4Na_2O_5$ (LeMont Productos Químicos, indicator grade) was achieved under sunlight irradiation (Fig. 1). The test was performed in a transparent borosilicate-glass bottle, with dimensions 2×10^{-3} m in thickness, 0.317 m in width and 0.072 m in diameter as a kind of SODIS technology. One coated strip was immersed into the bottle containing 750 mL of a solution of 50 mg L^{-1} of Eosin Y dye (Fig. 2). Before the bottle was exposed to sunlight irradiation, the system was placed in darkness for 60 min in order to achieve the adsorption–desorption equilibrium. The photoactivity degradation rate was recorded by measuring the intensity of the main absorption band of the Eosin Y (224 nm) as a function of the irradiation time. At given time intervals, samples were extracted and filtered through a 0.45 μm nylon filter and then monitored with an UV–vis spectrophotometer (Perkin Elmer Lambda 35). Solar irradiance and relative humidity data for the evaluation days was obtained from The Integrated Environmental Monitoring System (Sistema Integral de Monitoreo Ambiental, or SIMA) of Nuevo Leon State, Mexico.

3. Results and discussion

The physicochemical characteristics of Ag/TiO_2 and TiO_2 composites are summarized in Table 1. The X-ray diffraction spectra (XRD) of the bare semiconductors showed diffraction peaks for

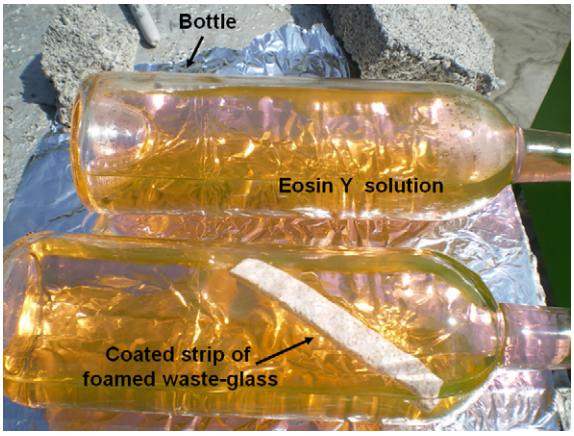

Fig. 2. Digital image during the course of solar photocatalytic degradation into a glass bottle of Eosin Y under irradiation of sunlight.

Table 1
Physicochemical properties of silver composites.

Sample	BET ($m^2\ g^{-1}$)	E_g (eV)	Anatase crystallite size[a] (nm)
P25 TiO_2	59	3.50	29
Ag/TiO_2	52	3.49	24

[a] From XRD.

TiO_2 anatase crystalline phase (JCPDF standard 21-1272) and rutile phase (JCPDF-70-7343). The presence of Ag° or AgO cannot be observed in the XRD patterns. Thus, it is possible to assume that Ag° particles may be highly dispersed on the TiO_2 surface and they cannot be detected by XRD due to their nanometric size and low concentration, 1 wt%. The titania crystallite dimensions for the semiconductors were calculated by using the Scherrer equation. These ranged from 29 nm for TiO_2 and 24 nm for Ag photodeposited onto TiO_2. Hence, both materials have about the same crystallite size. The specific surface area for the solids is also reported in Table 1. It is of the same order for the catalysts (59–52 $m^2\ g^{-1}$) and any effect of the silver incorporated to the TiO_2 cannot be observed. It can be seen that the band gap energy for the semiconductors as calculated from diffuse reflectance spectra using the Kubelka–Munk function, was not shifted as a consequence of the photodeposition of silver particles onto TiO_2. In general, both TiO_2 semiconductors have similar physicochemical properties, which will allow the study of the effect of silver on the solar dye oxidation. Additionally, FE-TEM images were obtained to determine the size of silver particles photodeposited onto the TiO_2 surface. In Fig. 3a and b silver particles of ~1.5 nm can be seen. For the titanium dioxide formed from Degussa P25 TiO_2, the interplanar distance measured by FFT on the image was ~0.3523 nm corresponding to its anatase phase (JCPDS standard 21-1272). Fig. 3b shows a FE-TEM image of a silver nanoparticle with an interplanar spacing measured by FFT of 0.2418 nm, corresponding approximately to Ag° phase according to the JCPDS standard 3-921. The particle size distributions were obtained from the HRTEM images; and they are presented in Fig. 3c. The silver particles on the composite were in average of 1.5 nm in diameter. The silver–TiO_2 nanocomposites have highly dispersed Ag° on a specific surface area of TiO_2 anatase support. These composites were coated over FWG strips. Foamed waste-glass is a recycled material made of waste bottles and others glasses with good absorption capacity for water [20] that makes it a good support for photocatalytic materials. For reference purpose, we listed the chemical composition of FWGS used to support the silver–TiO_2 composites, see Table 2. The strip is essentially composed of aluminosilicate. In FE-SEM images, Fig. 4, we observe that the surface of the strips is irregular with random macropores, which is due to surface roughness. It also has a low density (approximately 0.41–0.44 $g\ cm^{-3}$) and thus will float on water (light weight material). The morphology of TiO_2 and Ag/TiO_2 deposited on FWGS can be studied by the scanning electron microscopy (SEM) images. There are no differences; a representative FE-SEM image is shown in Fig. 4. The deposits are generally prepared in an ultrasonic environment, and are expected to be largely, the TiO_2 composition which has been confirmed by EDS analysis of the deposits (Fig. 4). We zoomed the sonochemical coating produced on the foamed waste-glass and these deposits were islands aggregated of TiO_2 quasi-spheres randomly dispersed onto the various sites on strips

Table 2
Chemical composition of foamed waste-glass.

	Composition						
	SiO_2	Al_2O_3	K_2O	Na_2O	Fe_2O_3	CaO	MgO
Weight (%)	74.0	15.0	4.5	4.5	1.2	0.5	0.3

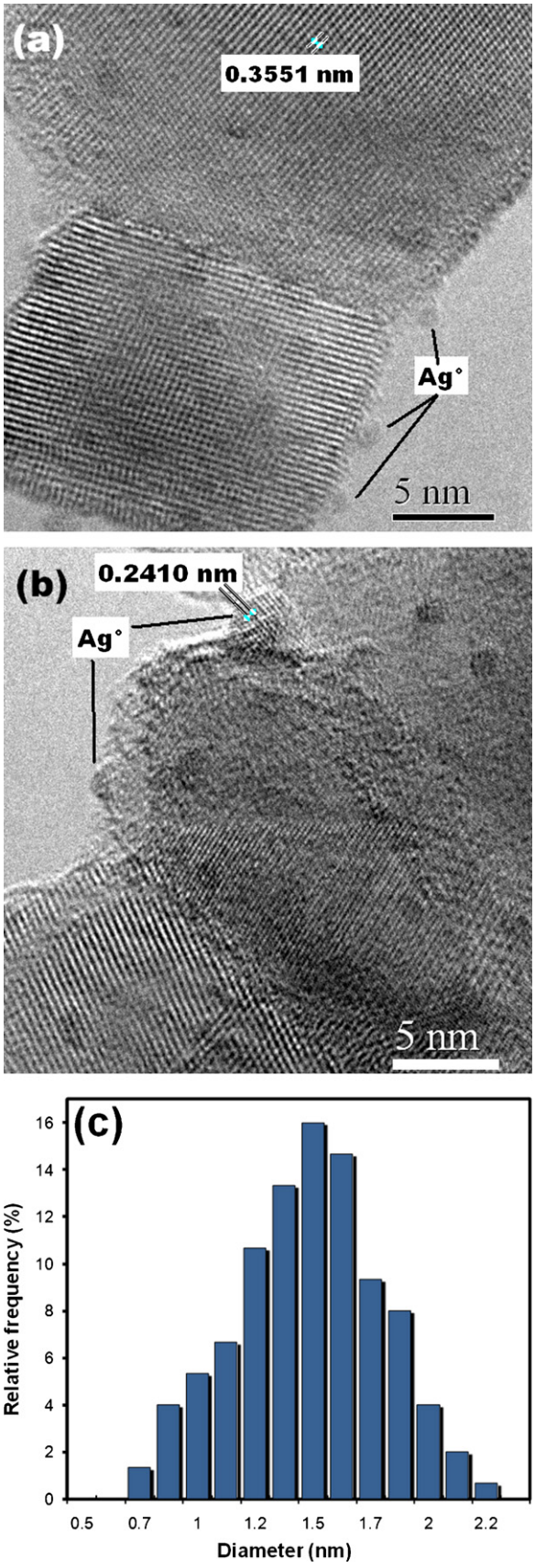

Fig. 3. (a and b) HRTEM images of silver photodeposited on TiO_2 P25; (c) particle size distribution for Ag/TiO_2.

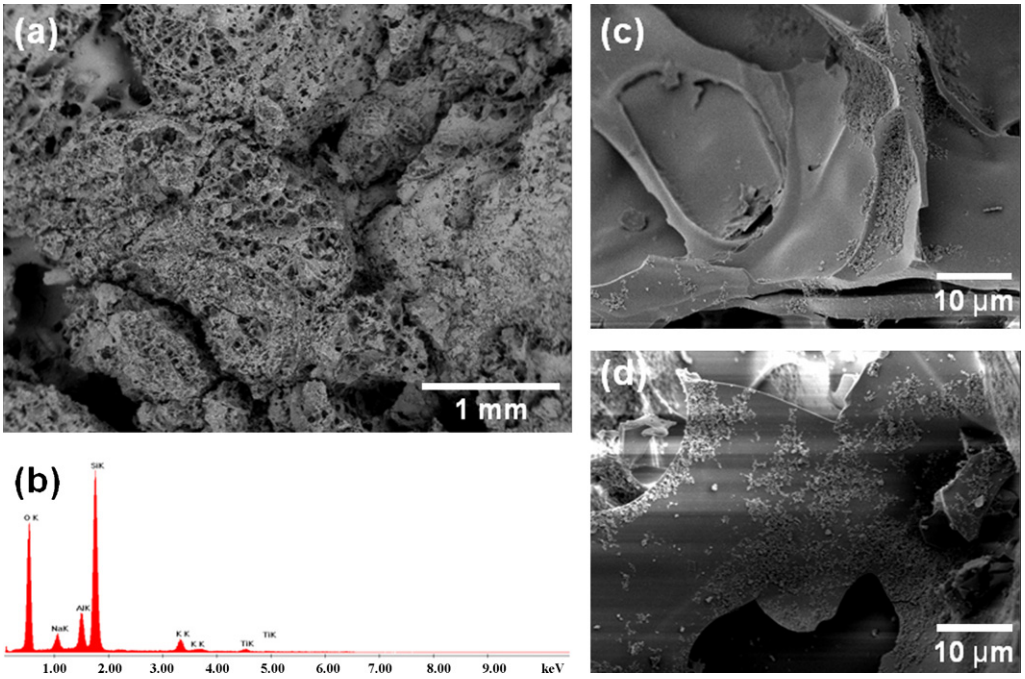

Fig. 4. FE-SEM images of (a) foamed waste-glass strip; (b) EDS spectra of coated FWGS and (c and d) Ag/TiO_2 deposited on FWGS.

(Fig. 4c and d). The deposits consist of quasi-spherical particles of around 25 nm in diameter (Fig. 5). The SEM image showing the morphology of film growth process, island structure growing in raised agglomeration (Fig. 5a and b) with identical morphology for both TiO_2 preparations and any effect of silver nanoparticles was not observed.

From the results showed above, we can say that TiO_2 and Ag/TiO_2 coated onto FWGS were successfully synthesized by an ultrasonic method in TiO_2 nanocomposite suspension in the presence of PVA surfactant. The mechanism of sonochemical deposition can be explained as follows: First, ultrasonic irradiation can help to disperse the TiO_2 particles. Next, the PVA surfactant inhibits the agglomeration of the particles and ultrasound produces its effects via the cavitation bubbles. These bubbles are generated during the sonication when the TiO_2 particles are highly dispersed generating tiny voids which collapse. Chemical activation for deposition is provided through the energy of the collapse of cavitation bubbles. The energy of the collapsing bubbles is so high as to produce oxidation, reduction, dissolution and decomposition [21]. The mechanism by which the silver nanocomposite nanoparticles are bonded to the FWG surface was reported by Pol et al. [21]. This mechanism is related to the microjets and shock waves created after the collapse of the bubbles. These jets, which cause the sintering of micron-sized metallic particles, push the nanoparticles toward the aluminosilicate surface at very high speeds. When they hit the FWGS surface, they can react with free Si–OH, Si–O–Si, or even Al–OH bonds. This may result in adhesion of the nanoparticles to the aluminosilicate surface. This technique seems to be a good option to prepare coated mixed oxides onto foamed waste-glass of low density, as an inexpensive technique which can work at room conditions. In addition, sonochemistry is a fast and efficient technique for coating [22]. Further experimental are currently conducted using different surfactants to understand the effect of the coated TiO_2 onto different foamed waste-glass substrates.

The FE-SEM images, as well as the EDS analysis confirm that the TiO_2 coating is achieved after 60 min. However, XRD of the strip does not allow us to determine if the TiO_2 anatase crystalline phase has changed to rutile phase during sonochemical process. Similar sonochemical studies reported that under sonication conditions, any change of the crystalline TiO_2 phases was not observed [22].

Solar irradiation in plastic PET bottles (SODIS) is a low-cost technology based on the solar exposure for some hours (normally 12 h) of commercial beverage bottles containing non-drinkable water [23]. In the photocatalytic evaluation of the coated FWGS, a glass bottle was used to reproduce the low-cost SODIS technology for photooxidation of Eosin yellow dye. The solar evaluations were

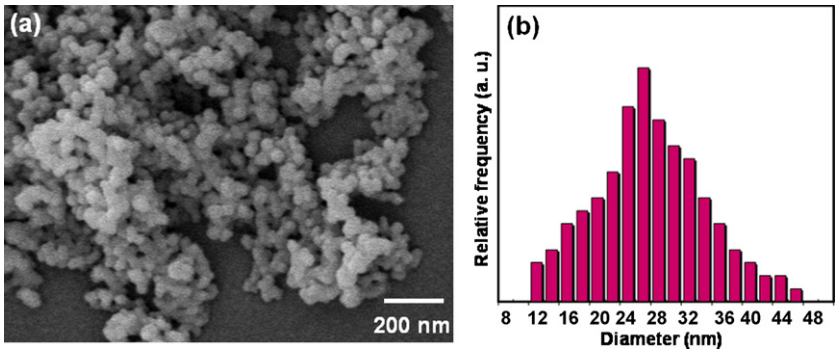

Fig. 5. (a) FE-SEM image of coat produced on a surface and (b) particle size distribution of quasi-sphere of raised deposit.

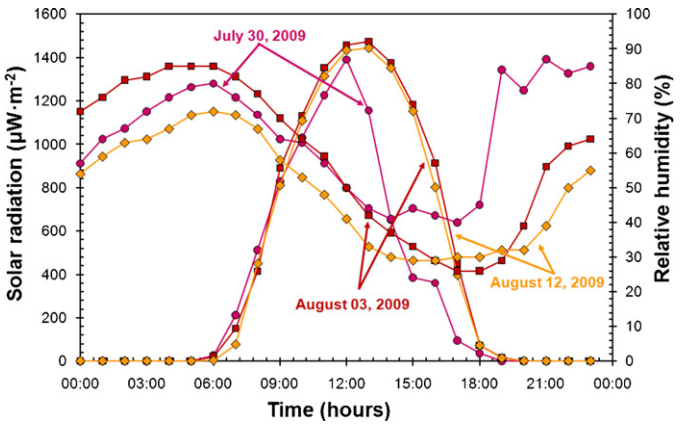

Fig. 6. Climate parameters for the days of solar evaluation in the city of Monterrey, México.

performed in the center of the city of Monterrey during summer time. In general, highest solar irradiance values are found in summer in Monterrey which are favorable for the solar photocatalytic evaluation. Fig. 6 shows the climate conditions on the days of the tests. It is clear that the irradiation and humidity were quite similar. So, the variations of these conditions were negligible for affecting photocatalytic activities.

The Eosin Y photocatalytic solar decomposition follows pseudo-first order kinetics, as shown in Fig. 7 for the two semiconductors coated on FWGS. The apparent rate constant K was calculated from the slope of the plot of $-\ln(C/C_0)$ versus time (Fig. 8 and Table 3). The corresponding activities are reported as half-life ($t_{1/2}$) in the same table. All the samples show more activity than photolysis ($t_{1/2}$ = 49 min) and it can be seen that the coated Ag/TiO_2 composite show the highest photoactivity. For the catalysts with Ag/TiO_2 coated on the FWGS, the half-life is 24 min and for the TiO_2-coated FWGS is 26 min. The performance of P25 TiO_2 is lower than that required for the Ag/TiO_2-coated FWGS. These results show that by incorporating coated TiO_2 or TiO_2–Ag composites onto the FWGS, solar photoactivity can be obtained. In comparison, complete UV photooxidation of Eosin Y is reached in an hour in the presence of TiO_2 (1 g L^{-1}) as reported by Poulios et al. [24]. Thus, it is significant that important decoloration is obtained for Eosin Y after 5 h under the natural solar irradiation in the summer in the city of Monterrey. For practical purposes, an evaluation of a suspension with Ag/TiO_2

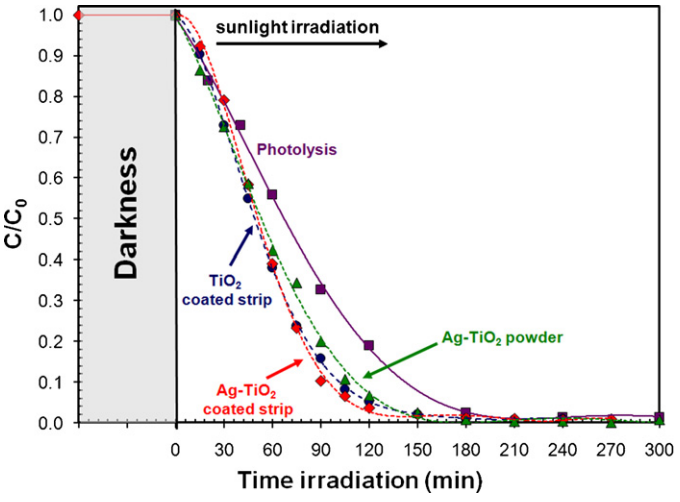

Fig. 7. Changes in Eosin Y concentration during the course of photocatalytic degradation of Eosin Y (50 mg L^{-1}) in the presence of TiO_2 and Ag/TiO_2-coated FWGS under sunlight irradiation.

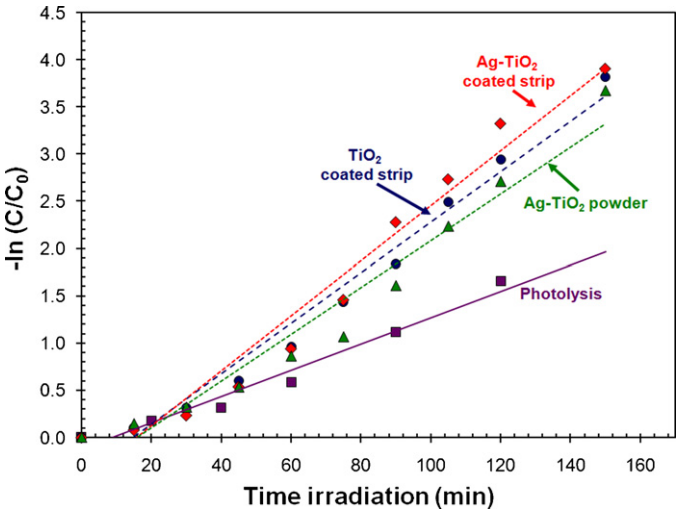

Fig. 8. Pseudo-first-order kinetics and apparent rate constant for the Eosin Y solar degradation.

Table 3
Kinetic parameters of the coated FWGS and slurry Eosin Y evaluations.

Sample	Reaction rate constant ($\times 10^{-2}$ min^{-1})	Half-life time (min)	TOC (mg L^{-1})	Mineralization (%)
Photolysis	1.4	49	11.1	36
TiO_2 P25 coated	2.6	26	10.5	39
Ag–TiO_2 coated	2.9	24	9.54	45
Ag–TiO_2 powder	2.5	28	8.61	50

in identical conditions to the FWGS evaluations was performed. Similar solar activity is shown from this test, with a $t_{1/2}$ of 28 min. However the conditions of this slurry experiment require continual recovery after filtration and drying of Ag/TiO_2 that represent additional work. Lixiviation of TiO_2 or Ag/TiO_2 from the FWGS was negligible.

However in Fig. 8, the apparent rate constants are similar and the effect of the different semiconductors is not clear. It seems that for silver nanocomposite the process is more direct, less organic intermediates are formed during the photocatalytic exposure. To know the percentage of mineralization of the slurry Ag/TiO_2 test, Ag/TiO_2-coated FWGS and titania-coated FWGS, an analysis of total organic carbon (TOC) analysis was determined with aliquots taken after 300 min. The calculated initial TOC value is 17.34 mg L^{-1}. Accordingly, determined values for Ag/TiO_2 slurry and coated on FWGS, the mineralization is greater compared with TiO_2 coated on FWGS (Table 3). However, both materials reach almost 50% of mineralization, while photolysis only achieved 36% of mineralization.

It is clear that silver–titania composite coating enhances the mineralization of Eosin Y. The possible reasons for this optimized performance may be due to the nanometric silver particles of ~1.5 nm in diameter that inhibit the accumulation of electrons on Ag° nanoparticles, resulting in a capture of electrons that improves the quick separation of charges. These effects can enhance the solar activity on the Eosin Y oxidation–mineralization. The immobilized system will be used for enhanced reusage of TiO_2 without any subsequent treatment. However, if the suspension of Ag/TiO_2 reaches the highest mineralization of Eosin Y, the slurry system is impractical for continuous processing.

4. Conclusions

The immobilization of Ag/TiO_2 and TiO_2 deposition on foamed waste-glass strips was achieved successfully by sonochemical

processing with polyvinyl alcohol as surfactant. The silver composites showed optimal photocatalytic activity for degradation of Eosin yellow dye under natural sunlight irradiation. The silver–titania composites show best performance with less intermediate organic molecule formation. This research offers a low-cost method to exploit highly efficient photocatalysts that can work under solar light irradiation. The suspension system is apparently more efficient that the immobilized system due to higher mass transfer and enhanced contact solid–liquid reactions. The immobilized system is more practical and economical since there is no need for treatment and filtration, as happens for slurry systems. It is significant that good decoloration–mineralization is obtained for Eosin Y after a few hours of irradiation under the natural solar irradiation in the summers of Monterrey city, México.

Acknowledgements

We thank Gladys Labrada Delgado and Daniel Ramírez González, microscopists of LINAN-IPICYT, for the SEM-TEM characterization of the materials studied in this work. We also thank J.A. Munguía-Tabares for valuable technical assistance in the experimental test during the program “Verano de la Ciencia, 2009-Academia Mexicana de las Ciencias”.

References

[1] K. Honda, A. Fujishima, Nature 238 (1972) 37.
[2] Z. Ding, G.Q. Lu, P.F. Greenfield, J. Phys. Chem. B 104 (2000) 4815.
[3] P.A. Pekakis, N.P. Xekoukoulotakis, D. Mantzavinos, Water Res. 40 (2006) 1276.
[4] S. Josset, J. Taranto, N. Keller, V. Keller, M.C. Lett, M.J. Ledoux, V. Bonnet, S. Rougeau, Catal. Today 129 (2007) 215.
[5] I.K. Konstantinou, V.A. Sakkas, T.A. Albanis, Appl. Catal. B 34 (2001) 227.
[6] A.D. Paola, G. Marci, L. Palmisano, M. Schiavello, K. Uosaki, S. Ikeda, B. Ohtani, J. Phys. Chem. B 106 (2002) 637.
[7] G. Colón, J.M. Sánchez-España, M.C. Hidalgo, J.A. Navío, J. Photochem. Photobiol. A 179 (2006) 20.
[8] G. Colón, M.C. Hidalgo, G. Munuera, I. Ferino, M.G. Cutrufello, J.A. Navío, Appl. Catal. B 63 (2006) 45.
[9] J. Moon, H. Takagi, Y. Fujishiro, M. Awano, J. Mater. Chem. 36 (2001) 949.
[10] O. Akhavan, J. Colloid Interface Sci. 336 (2009) 117.
[11] S. Anandan, P.S. Kumar, N. Pugazhenthiran, J. Madhavan, P. Maruthamuthu, Sol. Energy Mater. Sol. Cells 92 (2008) 929.
[12] R. van Grieken, J. Marugán, C. Sordo, P. Martínez, C. Pablos, Appl. Catal. B 93 (2009) 112.
[13] X. Yang, F. Ma, K. Li, Y. Guo, J. Hu, W. Li, M. Huo, Y. Guo, J. Hazard. Mater. 175 (2010) 429.
[14] J. Lonnen, S. Kilvington, S.C. Kehoe, F. Al-Touati, K.G. McGuigan, Water Res. 39 (2005) 877.
[15] S. Zhu, D. Zhang, X. Zhang, L. Zhang, X. Ma, Y. Zhang, M. Cai, Micropor. Mesopor. Mater. 126 (2009) 20.
[16] L. Sun, J. Li, C. Wang, S. Li, Y. Lai, H. Chen, C. Lin, J. Hazard. Mater. 171 (2009) 1045.
[17] D. Yang, S.E. Park, J.K. Lee, S.W. Lee, J. Cryst. Growth 311 (2009) 508.
[18] A. Gedanken, Ultrason. Sonochem. 11 (2004) 47.
[19] I. Perelshtein, G. Applerot, N. Perkas, G. Guibert, S. Mikhailov, A. Gedanken, Nanotechnology 19 (2008) 245705.
[20] J. Lu, K. Onitsuka, J. Environ. Sci. 16 (2004) 302.
[21] V.G. Pol, D.N. Srivastava, O. Palchik, V. Palchik, M.A. Slifkin, A.M. Weiss, A. Gedanken, Langmuir 18 (2002) 3352.
[22] K.V.P.M. Shafi, A. Ulman, X. Yan, N.-L. Yang, M. Himmelhaus, M. Grunze, Langmuir 17 (2001) 1726.
[23] B. Sommer, A. Mariño, Y. Solarte, M.L. Salas, C. Dierolf, C. Valiente, D. Mora, R. Rechteiner, J. Water Ser. Res. Technol.-Aqua 46 (1997) 127.
[24] I. Poulios, E. Micropoulou, R. Panou, E. Kostopoulou, Appl. Catal. B 41 (2003) 345.